

A scalable DG solver for the electroneutral Nernst-Planck equations

Thomas Roy*, Julian Andrej, Victor A. Beck

Lawrence Livermore National Laboratory, Livermore, 94550, CA, USA

Abstract

The robust, scalable simulation of flowing electrochemical systems is increasingly important due to the synergy between intermittent renewable energy and electrochemical technologies such as energy storage and chemical manufacturing. The high Péclet regime of many such applications prevents the use of off-the-shelf discretization methods. In this work, we present a high-order Discontinuous Galerkin scheme for the electroneutral Nernst-Planck equations. The chosen charge conservation formulation allows for the specific treatment of the different physics: upwinding for advection and migration, and interior penalty for diffusion of ionic species as well the electric potential. Similarly, the formulation enables different treatments in the preconditioner: AMG for the potential blocks and ILU-based methods for the advection-dominated concentration blocks. We evaluate the convergence rate of the discretization scheme through numerical tests. Strong scaling results for two preconditioning approaches are shown for a large 3D flow-plate reactor example.

Keywords: Electrochemical flow, Nernst-Planck, Electroneutrality, Discontinuous Galerkin, Preconditioning

2010 MSC: 65N30, 65F08, 78A57

1. Introduction

With the steady transition to renewable energy comes a surge of intermittent electricity [1, 2]. Fortunately, various electrochemical technologies such as energy storage and electrochemical manufacturing can capitalize on this otherwise wasted energy [3, 4]. To handle the rise of renewable energy, the development and scaling-up of these technologies is crucial. Naturally, this brings a need for simulation to aid design of electrochemical devices at the industrial scale.

Such simulations require the solution of highly coupled systems of partial differential equations (PDEs). An important model in the presence of fluid

*Corresponding author

Email addresses: roy27@llnl.gov (Thomas Roy), andrej1@llnl.gov (Julian Andrej), beck33@llnl.gov (Victor A. Beck)

flow is the Nernst-Planck (NP) equation, which describes the transport of an ionic species by advection, diffusion and electromigration [5]. For multi-ion transport, the system consisting of an NP equation for each species can be closed by a Poisson equation for the electric potential. However, the Poisson equation operates on a much smaller lengthscale and is thus challenging to solve computationally [6]. Due to the scale separation, it is commonly replaced by the electroneutrality condition: an algebraic equation for the ionic concentrations.

For the electroneutral system, arriving at a steady-state solution is a challenging numerical task and therefore the discretization scheme has to be chosen with care. In particular, specific treatment is required for the typically advection-dominated nature of the flow. The considered physical equations have been successfully discretized with several methods in the past. The authors in [7] use a multi-dimensional upwinding method similar to a finite volume approach. A continuous Galerkin finite element method has to employ a stabilization scheme because of the advection-dominated system, which was shown in [8] using a Variational Multiscale Method. There have been attempts at one-dimensional problems using the Discontinuous Galerkin (DG) Method [9, 10], which showed promising results and motivated this research. To the best of the authors' knowledge, none of the previously mentioned references looked into the benefits of high-order DG spatial discretizations, which are frequently used in advection-dominated transport and compressible flow applications [11].

After discretization and linearization, large, sparse linearized systems must be solved. Iterative methods using appropriate preconditioning techniques [12] are key to obtaining a scalable solver. Designing preconditioners for problems with several, simultaneous, coupled physical phenomena is especially challenging since different parts of the problem may require different treatments. In the case of electroneutral ion transport, the equations are elliptic with respect to the electrical potential but hyperbolic with respect to the concentration variables. Scalable solvers for this problem are not available in commercial tools, where direct solver are used. This is especially restrictive when aiming for industrial scale 3D simulations, as well as the simulation of porous electrodes at the resolved pore-scale.

In this paper, we present a high-order DG spatial discretization and scalable preconditioning approaches for the electroneutral Nernst-Planck equations. The electroneutral system is arranged in a charge-conservation formulation that is necessary for the proper penalization of the potential terms in the DG scheme. Additionally, this formulation also allows for block preconditioning with specific treatment of the potential block and concentration blocks.

In section 2, the equations for the relevant electrochemical physics in an electroneutral setting are described. We explain how to reorder the equations and exploit the electroneutrality condition to eliminate a species variable and construct the charge conservation equation. Next, in section 3, we detail the spatial discretization process using the DG finite element method including necessary treatment for the hyperbolic and elliptic parts of the resulting system. Then, in section 4, we outline our approach to numerically precondition and solve the resulting discrete nonlinear problem. Finally, in section 5, we perform

a convergence test for our discrete scheme and show scaling results for a large three-dimensional, industry-relevant problem.

2. Governing Equations

We consider the equations for electroneutral multi-ion transport. First, we describe the standard Electroneutral-Nernst-Planck model, as well as appropriate boundary conditions for a flow-plate reactor. Then, we discuss alternative formulations including the Charge-Conservation-Nernst-Planck model, which will be used for our Discontinuous Galerkin scheme in section 3. A nondimensionalization of that model is also given.

2.1. Electroneutral Nernst-Planck equation

We consider the flow of a dilute electrolyte solution containing $m \geq 2$ chemical species in a domain $\Omega \in \mathbb{R}^d$, $d = 1, 2$, or 3 . In the presence of an electric field, the mass transport is described by the Nernst-Planck equation [5]. For simplicity, we do not consider the transient case, although our approach would still be applicable.

At steady state, the conservation of mass of each species $k = 1, \dots, m$ is given by

$$-\nabla \cdot (D_k \nabla c_k) + \nabla \cdot (c_k \mathbf{u}) - \nabla \cdot (z_k \mu_k F c_k \nabla \Phi) - R_k = 0 \quad \text{in } \Omega, \quad (1)$$

where c_k is the molar concentration of species k , D_k is the molecular diffusion coefficient, \mathbf{u} is the velocity of the electrolyte, z_k is the valence (charge number), μ_k is the mobility constant, F is the Faraday constant, Φ is the electric potential in the electrolyte, and R_k is a reaction term. The first term in (1) describes molecular diffusion, the second, advection, and the third, electromigration.

The mobility constant is given by the Nernst-Einstein relation [5]

$$\mu_k = \frac{D_k}{RT}, \quad (2)$$

where R is the universal gas constant, and T is the thermodynamic temperature.

The system currently consists of m equations (1), and $m + 1$ unknowns: the m concentrations c_k and the potential Φ . An additional equation is required to complete the system. A commonly-used relation is the electroneutrality approximation

$$\sum_{k=1}^m z_k c_k = 0 \quad \text{in } \Omega, \quad (3)$$

which states that there is no charge separation and that neutrality is maintained everywhere. This approximation is obtained from the Poisson equation and is appropriate when considering length scales greater than nanometers [6].

In [8], the system consisting of (1) and (3) is called the Electroneutrality-Nernst-Planck (ENP) model.

For convenience, we denote the advection-migration transport as $\mathbf{q}_k = \mathbf{u} - z_k \mu_k F \nabla \Phi$ so that (1) can be written as

$$-\nabla \cdot (D_k \nabla c_k) + \nabla \cdot (c_k \mathbf{q}_k) - R_k = 0 \quad \text{in } \Omega. \quad (4)$$

We now provide boundary conditions that are appropriate for a flow plate reactor. The boundary $\partial\Omega$ is partitioned with respect to the direction of the velocity at the boundary into the inlet boundary Γ_{in} , the outlet boundary Γ_{out} , the wall boundary Γ_{wall} and the electrode boundary Γ_{elec} . We have

$$\begin{aligned} \Gamma_{\text{in}} &= \{\mathbf{x} \in \partial\Omega \mid \mathbf{u} \cdot \mathbf{n} < 0\}, \\ \Gamma_{\text{out}} &= \{\mathbf{x} \in \partial\Omega \mid \mathbf{u} \cdot \mathbf{n} > 0\}, \\ \Gamma_{\text{wall}} \cup \Gamma_{\text{elec}} &= \{\mathbf{x} \in \partial\Omega \mid \mathbf{u} \cdot \mathbf{n} = 0\}, \end{aligned}$$

where \mathbf{n} is the outward normal, so that $\partial\Omega = \Gamma_{\text{in}} \cup \Gamma_{\text{out}} \cup \Gamma_{\text{wall}} \cup \Gamma_{\text{elec}}$. Each boundary is such that $\Gamma_i \cap \Gamma_j = \emptyset$. The location of the wall and electrode boundaries are determined beforehand.

The boundary conditions are given by

$$(c_k \mathbf{q}_k - D_k \nabla c_k) \cdot \mathbf{n} = c_k^{\text{in}} \mathbf{u} \cdot \mathbf{n} \quad \text{on } \Gamma_{\text{in}}, \quad (5)$$

$$(D_k \nabla c_k + z_k \mu_k F c_k \nabla \Phi) \cdot \mathbf{n} = 0 \quad \text{on } \Gamma_{\text{out}}, \quad (6)$$

$$(D_k \nabla c_k + z_k \mu_k F c_k \nabla \Phi) \cdot \mathbf{n} = g_k \quad \text{on } \Gamma_{\text{elec}}, \quad (7)$$

$$(D_k \nabla c_k + z_k \mu_k F c_k \nabla \Phi) \cdot \mathbf{n} = 0 \quad \text{on } \Gamma_{\text{wall}}, \quad (8)$$

where g_k represents electrochemical reactions at the electrode surface.

In our numerical experiments, we will consider the specific case of a simple n -electron transfer redox reaction $Ox + ne^- \rightarrow Red$, where the current density J_n at the electrodes is given by the Butler-Volmer equation

$$J_n = J_0 \left[\left(\frac{c_r}{c_r^*} \right)^\gamma \exp \left(\alpha_1 \frac{nF}{RT} (\Phi_{\text{app}} - \Phi) \right) - \left(\frac{c_o}{c_o^*} \right)^\gamma \exp \left(-\alpha_2 \frac{nF}{RT} (\Phi_{\text{app}} - \Phi) \right) \right], \quad (9)$$

where J_0 is the exchange current density, c_o and c_r are the concentrations of the oxidant Ox and reductant Red , respectively, c_o^* and c_r^* are reference concentrations, α_1 and α_2 are the anodic and cathodic charge transfer coefficients, respectively, n is the number of electrons in the reaction, and Φ_{app} is the applied potential. The reaction rate in (7) is given by $g_k = \frac{J_n}{nF}$ if k is the oxidant, $g_k = -\frac{J_n}{nF}$ if it is the reductant, and $g_k = 0$ otherwise.

2.2. Alternative formulations

Alternative formulations of the ENP system (1) and (3) have different advantages with respect to the numerical solution [8].

In our case, we are interested in the Discontinuous Galerkin (DG) finite element method [13]. In particular, we will consider upwinding techniques for the advection and migration terms. The current formulation, ENP, is problematic with respect to the stabilization and penalization of the potential Φ . Indeed, the mass conservation equations (1) will be treated as transport problems for the concentrations, using an upwinding scheme, leaving Φ untreated. In this electroneutral Nernst-Planck system, the electroneutrality approximation replaces the Poisson equation, where stabilization and penalization appropriate for an elliptic problem could have been used. We need an equation that plays this role for Φ .

We formulate a charge conservation equation by summing over all conservation of mass equations (1) weighting each by $z_k F$. The advection terms cancel due to electroneutrality (3), and we obtain

$$-F \nabla \cdot \left[\sum_{k=1}^m z_k D_k \nabla c_k \right] - \nabla \cdot \left[\left(\sum_{k=1}^m z_k^2 \mu_k F^2 c_k \right) \nabla \Phi \right] - \sum_{k=1}^m z_k F R_k = 0 \quad \text{in } \Omega. \quad (10)$$

However, we note that the system consisting of (1) and (10) is linearly dependent. To circumvent this, one of the concentration unknowns can be eliminated using the electroneutrality condition. Without loss of generality, we eliminate the concentration c_m using the substitution

$$c_m = -\frac{1}{z_m} \sum_{k=1}^{m-1} z_k c_k, \quad (11)$$

assuming that $z_m \neq 0$. Combining (10) and (11), we obtain

$$-F \nabla \cdot \left[\sum_{k=1}^{m-1} z_k (D_k - D_m) \nabla c_k \right] - \nabla \cdot \left[\left(\sum_{k=1}^{m-1} z_k (z_k \mu_k - z_m \mu_m) F^2 c_k \right) \nabla \Phi \right] - \sum_{k=1}^{m-1} z_k F R_k = 0 \quad \text{in } \Omega. \quad (12)$$

This conservation of charge equation replaces the conservation of mass of species m in the system. The system now consists of m equations: conservation of mass equations (1) for $k = 1, \dots, m-1$, and a conservation of charge equation (12), and m unknowns: concentration unknowns c_k for $k = 1, \dots, m-1$, and the electric potential Φ . As in [8], we call this formulation the Charge-conservation-Nernst-Planck (CNP) model.

In terms of the DG scheme, stabilization and penalization of c_m is no longer needed since it is no longer an unknown of the system. We can instead treat (12) as an elliptic equation for Φ in terms of the DG stabilization and penalization.

2.3. Nondimensionalization

Here we perform a nondimensionalization of the CNP model consisting of (1) and (10) and boundary conditions (5) to (8). Note that this scaling process generally helps numerical algorithms. Indeed, for the considered test cases, this greatly accelerates the convergence of the iterative methods.

Let the following nondimensional variables:

$$\hat{\Phi} = \frac{F}{RT}\Phi, \quad \hat{c}_k = \frac{c_k}{c_k^{\text{in}}}, \quad \hat{\mathbf{x}} = \frac{1}{L}\mathbf{x}, \quad \hat{\mathbf{u}} = \frac{1}{u_{\text{avg}}}\mathbf{u}, \quad (13)$$

and the differential operator with respect $\hat{\mathbf{x}}$

$$\hat{\nabla} = L\nabla. \quad (14)$$

Substituting (13) and (14) into (1), we obtain

$$-\hat{\nabla} \cdot (\hat{D}_k \hat{\nabla} \hat{c}_k) + \hat{\nabla} \cdot (\hat{c}_k \hat{\mathbf{u}}) - \hat{\nabla} \cdot (z_k \hat{D}_k \hat{c}_k \hat{\nabla} \hat{\Phi}) - \frac{L}{c_k^{\text{in}} u_{\text{avg}}} R_k = 0 \quad \text{in } \Omega, \quad (15)$$

where $\hat{D}_k = \frac{D_k}{L u_{\text{avg}}}$ is the inverse Péclet number. We note that the electroneutrality condition (3) is now

$$\sum_{k=1}^m z_k c_k^{\text{in}} \hat{c}_k = 0, \quad (16)$$

so that \hat{c}_m is eliminated using

$$\hat{c}_m = -\frac{1}{z_m c_m^{\text{in}}} \sum_{k=1}^{m-1} z_k c_k^{\text{in}} \hat{c}_k. \quad (17)$$

In order to nondimensionalize the charge conservation equation (10), we introduce the reference concentration c_{ref} to obtain

$$\begin{aligned} -\hat{\nabla} \cdot \left[\sum_{k=1}^m z_k \hat{D}_k \frac{c_k^{\text{in}}}{c_{\text{ref}}} \hat{\nabla} \hat{c}_k \right] - \hat{\nabla} \cdot \left[\left(\sum_{k=1}^m z_k^2 \hat{D}_k \frac{c_k^{\text{in}}}{c_{\text{ref}}} \hat{c}_k \right) \hat{\nabla} \hat{\Phi} \right] \\ - \sum_{k=1}^m \frac{L}{c_{\text{ref}} u_{\text{avg}}} z_k R_k = 0 \quad \text{in } \Omega. \end{aligned} \quad (18)$$

The boundary conditions (5) to (8) become

$$(\hat{c}_k \hat{\mathbf{q}}_k - \hat{D}_k \hat{\nabla} \hat{c}_k) \cdot \mathbf{n} = \hat{\mathbf{u}} \cdot \mathbf{n} \quad \text{on } \Gamma_{\text{in}}, \quad (19)$$

$$(\hat{D}_k \hat{\nabla} \hat{c}_k + z_k \hat{D}_k \hat{c}_k \hat{\nabla} \hat{\Phi}) \cdot \mathbf{n} = 0 \quad \text{on } \Gamma_{\text{out}}, \quad (20)$$

$$(\hat{D}_k \hat{\nabla} \hat{c}_k + z_k \hat{D}_k \hat{c}_k \hat{\nabla} \hat{\Phi}) \cdot \mathbf{n} = \frac{1}{u_{\text{avg}} c_k^{\text{in}}} g_k \quad \text{on } \Gamma_{\text{elec}}, \quad (21)$$

$$(\hat{D}_k \hat{\nabla} \hat{c}_k + z_k \hat{D}_k \hat{c}_k \hat{\nabla} \hat{\Phi}) \cdot \mathbf{n} = 0 \quad \text{on } \Gamma_{\text{wall}}. \quad (22)$$

In the specific case of the Butler-Volmer equation (9), if k is an oxidant, (21) becomes

$$(\hat{D}_k \hat{\nabla} \hat{c}_k + z_k \hat{D}_k \hat{c}_k \hat{\nabla} \hat{\Phi}) \cdot \mathbf{n} = \hat{J}_0 \left[\left(\hat{c}_r \frac{c_r^{\text{in}}}{c_r^*} \frac{c_k^*}{c_k^{\text{in}}} \right)^\gamma \exp(\hat{\Phi}_{\text{app}} - \hat{\Phi}) - \hat{c}_k^\gamma \exp(-(\hat{\Phi}_{\text{app}} - \hat{\Phi})) \right], \quad (23)$$

$$\text{where } \hat{J}_0 = \frac{J_0 (c_k^{\text{in}})^{\gamma-1}}{u_{\text{avg}} F (c_k^*)^\gamma} \text{ and } \hat{\Phi}_{\text{app}} = \frac{F}{RT} \Phi_{\text{app}}.$$

3. Discontinuous Galerkin method

In this section, we introduce a Discontinuous Galerkin (DG) scheme for the CNP model (4) and (12). After reviewing preliminary DG concepts, we provide DG schemes for a hyperbolic and an elliptic equation. The resulting numerical fluxes are then used for the full system (4) and (12). For generality, we provide the scheme for the dimensional equations instead of the nondimensionalized version from section 2.3.

3.1. Preliminaries

We begin by introducing the appropriate functional notation. Let \mathcal{T}_h be a subdivision of Ω with element $K \in \mathcal{T}_h$. The broken Sobolev spaces are defined as

$$H^l(\mathcal{T}_h) = \{v \in L^2(\Omega) : v|_K \in H^l(K)\}. \quad (24)$$

Let $\Gamma = \cup_{K \in \mathcal{T}_h} \partial K$ denote the set of element boundaries. The restrictions of functions in $H^1(\mathcal{T}_h)$ to Γ are called *traces* and belong to the function space $T(\Gamma) = \Pi_{K \in \mathcal{T}_h} L^2(\partial K)$.

Denote the space of polynomials of degree p on each element κ with Q^p . A proper finite element space is defined as

$$V_h^p = \{v_h \in L^2(\Omega) : v_h|_K \in Q^p\}. \quad (25)$$

Next we introduce some trace operators needed for the numerical fluxes. For $u \in T(\Gamma)$, we define the average $\{u\}$ and jump $[[u]]$ on interior faces as

$$\{u\} = \frac{1}{2}(u^- + u^+), \quad [[u]] = u^- \mathbf{n}^- + u^+ \mathbf{n}^+ \quad \text{on } e \in \mathcal{E}^\circ, \quad (26)$$

and for $\mathbf{q} \in [T(\Gamma)]^d$,

$$\{\mathbf{q}\} = \frac{1}{2}(\mathbf{q}^- + \mathbf{q}^+), \quad [[\mathbf{q}]] = \mathbf{q}^- \cdot \mathbf{n}^- + \mathbf{q}^+ \cdot \mathbf{n}^+ \quad \text{on } e \in \mathcal{E}^\circ. \quad (27)$$

Jumps on exterior faces are defined as

$$[[u]] = u\mathbf{n}, \quad \{\mathbf{u}\} = \mathbf{u} \quad \text{on } e \in \mathcal{E}^\Gamma. \quad (28)$$

3.2. Applied to the CNP model

Following a combination of [14, 15, 16], we derive a Discontinuous Galerkin formulation for the CNP model. In this section, we only consider zero-Dirichlet boundary conditions for simplicity. The full scheme with boundary conditions (5) to (8) is given in section 3.3.

Analyzing (4) we can see that it consists of a diffusion, advection-migration, and reaction term. Each term has to be treated carefully in order to achieve a convergent DG discretization.

We multiply (4) by a test function v and integrate over the domain Ω .

$$-\int_{\Omega} \nabla \cdot (D_k \nabla c_k) v \, dx + \int_{\Omega} \nabla \cdot (c_k \mathbf{q}_k) v \, dx - \int_{\Omega} R_k v \, dx = 0 \quad \text{in } \Omega. \quad (29)$$

The diffusion term can be treated exactly like in [16] with the appropriate flux choices

$$\hat{c}_k = \{c_k\} \text{ on } \Gamma_I, \quad \hat{c}_k = 0 \text{ on } \partial\Omega, \quad \hat{\sigma} = \{\nabla c_k\} - D_k \delta_p \llbracket c_k \rrbracket \text{ on } \Gamma, \quad (30)$$

where δ_p is a penalty parameter that depends on the polynomial order p of the finite elements. In [11], it is given by

$$\delta_p = C_{\text{IP}} \frac{p^2}{h}, \quad (31)$$

where $C_{\text{IP}} > 0$ needs to be large enough for stability, and h is the cell diameter. The diffusion term results in

$$\begin{aligned} & -\int_{\Omega} \nabla \cdot (D_k \nabla c_k) v \, dx \approx \\ & \int_{\Omega} D_k \nabla c_k \cdot \nabla v \, dx - \int_{\Gamma} D_k (\llbracket c_k \rrbracket \cdot \{\nabla v\} + \{\nabla c_k\} \cdot \llbracket v \rrbracket) \, ds + \int_{\Gamma} D_k \delta_p \llbracket c_k \rrbracket \cdot \llbracket v \rrbracket \, ds. \end{aligned} \quad (32)$$

The advection-migration term combines the advection effect from the transport velocity \mathbf{v} and the migration effect from the potential gradient $\nabla \Phi$, which can be treated with the combined variable \mathbf{q}_k . This combined term is treated as in [15] with the upwind flux, resulting in

$$\begin{aligned} & \int_{\Omega} \nabla \cdot (c_k \mathbf{q}_k) v \, dx \approx \\ & -\int_{\Omega} c_k \mathbf{q}_k \cdot \nabla v \, dx + \int_{\Gamma_I} \left(\{c_k \mathbf{q}_k\} + \frac{|\mathbf{q}_k \cdot \mathbf{n}|}{2} \llbracket c_k \rrbracket \right) \cdot \llbracket v \rrbracket \, ds. \end{aligned} \quad (33)$$

Since the reaction term is cell-local, and it is assumed not to contain derivatives of the primary solution variables, no further treatment is needed.

Note that the gradient potential term $\nabla \Phi$ in the mass conservation equations (4) is only treated like a velocity in an advective term for the concentrations.

A penalty term is required for the stability of the DG scheme and that is why we are using the CNP model. Indeed, the gradient potential term in the charge conservation equation (12) will be treated like an elliptic term, with appropriate penalization. Conversely, since we have already penalized the concentration gradients ∇c_k in our treatment of (4), it is not required to do so for (12).

We introduce the following short-hand notation for (12)

$$a_{km} = Fz_k(D_k - D_m), \quad (34)$$

$$\kappa = \sum_{k=1}^{m-1} z_k(z_k\mu_k - z_m\mu_m)F^2, \quad (35)$$

$$f = \sum_{k=1}^m z_kFR_k, \quad (36)$$

which results in

$$-\nabla \cdot \left[\sum_{k=1}^{m-1} a_{km} \nabla c_k \right] - \nabla \cdot (\kappa \nabla \Phi) - f = 0 \quad \text{in } \Omega. \quad (37)$$

The fluxes for the concentration term are chosen as

$$\hat{c}_k = \{c_k\} \text{ on } \Gamma_I, \quad \hat{c}_k = 0 \text{ on } \partial\Omega, \quad \hat{\sigma} = \{\nabla c_k\} \text{ on } \Gamma. \quad (38)$$

Without loss of generality, the case with only two species in the system ($k = 2$) results in

$$\int_{\Omega} a_1 \nabla c_1 \cdot \nabla v \, dx - \int_{\Gamma} a_1 (\llbracket c_1 \rrbracket \cdot \{\nabla v\} + \{\nabla c_1\} \cdot \llbracket v \rrbracket) \, ds = \int_{\Omega} f v \, dx, \quad (39)$$

where $a_1 = a_{12}$. For the potential term, we choose fluxes with interior penalty

$$\hat{\Phi} = \{\Phi\} \text{ on } \Gamma_I, \quad \hat{\Phi} = 0 \text{ on } \partial\Omega, \quad \hat{\sigma} = \{\kappa \nabla \Phi\} - \{\kappa\} \delta_p \llbracket \Phi \rrbracket \text{ on } \Gamma. \quad (40)$$

This results in

$$\begin{aligned} \int_{\Omega} \kappa \nabla \Phi \cdot \nabla v \, dx - \int_{\Gamma} (\llbracket \Phi \rrbracket \cdot \{\kappa \nabla v\} + \{\kappa \nabla \Phi\} \cdot \llbracket v \rrbracket) \, ds \\ + \int_{\Gamma} \{\kappa\} \delta_p \llbracket \Phi \rrbracket \cdot \llbracket v \rrbracket \, ds = \int_{\Omega} f v \, dx, \end{aligned} \quad (41)$$

with the standard symmetric interior penalty flux. Note that in this example we assume the same test function space for all concentrations c_k and the potential Φ . Therefore, we use the same penalty parameter δ_p . If the polynomial spaces have different orders, the penalty parameters for both terms should be chosen accordingly. In our numerical experiments, we use (31) with $C_{IP} = 10$.

3.3. Scheme

Let the short-hand notation for the current at the electrode boundary

$$g = \sum_{k=1}^m z_k F g_k, \quad (42)$$

where g_k are the reaction rates from (7).

The DG scheme for the problem eqs. (4) to (8) and (12) is given by: Find $c_k \in V_h^p$ for $k = 1, \dots, m-1$, and $\Phi \in V_h^p$ such that

$$\begin{aligned} & \int_{\Omega} D_k \nabla c_k \cdot \nabla v_k \, dx - \int_{\Gamma_I} ([c_k] \cdot \{D_k \nabla v_k\} + \{D_k \nabla c_k\} \cdot [v_k]) \, ds \\ & \quad + \int_{\Gamma_I} \{D_k\} \delta_p [c_k] \cdot [v_k] \, ds - \int_{\Omega} c_k \mathbf{q}_k \cdot \nabla v_k \, dx \\ & \quad + \int_{\Gamma_I} \left(\{c_k \mathbf{q}_k\} + \frac{|\mathbf{q}_k \cdot \mathbf{n}|}{2} [c_k] \right) \cdot [v_k] \, ds + \int_{\Gamma_{\text{out}}} (\mathbf{q}_k \cdot \mathbf{n}) c_k v_k \, ds \\ & \quad + \int_{\Gamma_{\text{in}}} (\mathbf{u} \cdot \mathbf{n}) c_k^{\text{in}} v_k \, ds - \int_{\Gamma_{\text{elec}}} g_k v_k \, ds - \int_{\Omega} R_k v_k \, dx = 0, \quad (43a) \end{aligned}$$

for all $v_k \in V_h^p$, for $k = 1, \dots, m-1$, and

$$\begin{aligned} & \sum_{k=1}^{m-1} \left[\int_{\Omega} a_{km} \nabla c_k \cdot \nabla v_m \, dx - \int_{\Gamma_I} ([c_k] \cdot \{a_{km} \nabla v_m\} + \{a_{km} \nabla c_k\} \cdot [v_m]) \, ds \right] \\ & \quad + \int_{\Omega} \kappa \nabla \Phi \cdot \nabla v_m \, dx - \int_{\Gamma_I} ([\Phi] \cdot \{\kappa \nabla v_m\} + \{\kappa \nabla \Phi\} \cdot [v_m]) \, ds \\ & \quad + \int_{\Gamma_I} \{\kappa\} \delta_p [\Phi] \cdot [v_m] \, ds - \int_{\Gamma_{\text{elec}}} g v_m \, ds - \int_{\Omega} f v_m \, dx = 0, \quad (43b) \end{aligned}$$

for all $v_m \in V_h^p$.

Recall that the eliminated concentration c_m can be recovered from the substitution (11). Note that in (43b), the inlet boundary conditions cancel due to electroneutrality.

4. Numerical details and preconditioning

A crucial aspect in the practical usability of this specific discretization is the ability to solve it efficiently when applied to real world problems. Domains for such applications are usually three-dimensional and nonlinear couplings appear through species reactions. Consequently, the numerical solution approach has to be scalable on a desired hardware architecture to provide feasible turnaround times for experiments. As a first performance measure, we are focusing on hexahedral mesh elements, which allow for a tensor product element approach [17], a fact that we exploit in our implementation (note that we are not exploiting

Gauss-Legendre-Lobatto nodes, because we tend to use higher-order quadrature rules compared to the polynomial degree).

After discretization, the nonlinear system arising from (43) has to be linearized and solved frequently. To solve the nonlinear system, we employ a Newton method along with backtracking linesearch [18]. To ensure a scalable linear solving procedure we have to employ appropriate preconditioning techniques [12].

We can rewrite (43) as a block residual equation

$$\mathcal{R} = \begin{bmatrix} R_\Phi \\ R_{c_1} \\ \vdots \\ R_{c_{m-1}} \end{bmatrix} = 0,$$

where R_Φ is the residual of the discretized charge conservation equation (43b), and R_{c_i} , $i = 1, \dots, m-1$, correspond to the residuals of the mass conservation equations (43a). Linearization of the residual \mathcal{R} results in the block matrix

$$\begin{aligned} J = \frac{\partial \mathcal{R}}{\partial(\Phi, c_1, \dots, c_{m-1})} &= \begin{bmatrix} \frac{\partial R_\Phi}{\partial \Phi} & \frac{\partial R_\Phi}{\partial c_1} & \cdots & \frac{\partial R_\Phi}{\partial c_{m-1}} \\ \frac{\partial R_{c_1}}{\partial \Phi} & \frac{\partial R_{c_1}}{\partial c_1} & \cdots & \frac{\partial R_{c_1}}{\partial c_{m-1}} \\ \vdots & \vdots & \ddots & \vdots \\ \frac{\partial R_{c_{m-1}}}{\partial \Phi} & \frac{\partial R_{c_{m-1}}}{\partial c_1} & \cdots & \frac{\partial R_{c_{m-1}}}{\partial c_{m-1}} \end{bmatrix} \\ &= \begin{bmatrix} A_{\Phi\Phi} & A_{\Phi c_1} & \cdots & A_{\Phi c_{m-1}} \\ A_{c_1\Phi} & A_{c_1 c_1} & \cdots & A_{c_1 c_{m-1}} \\ \vdots & \vdots & \ddots & \vdots \\ A_{c_{m-1}\Phi} & A_{c_{m-1} c_1} & \cdots & A_{c_{m-1} c_{m-1}} \end{bmatrix}. \end{aligned} \quad (44)$$

This block system is used in the following sections to determine preconditioning strategies.

4.1. Preconditioning for $p = 1$

We first describe the preconditioning strategy for a piecewise linear discretization.

When dealing with block systems resulting from the discretizations of systems of PDEs with different underlying physics, it is usually not sufficient and never optimal to use the same preconditioner for each block. Analyzing the linearized block system (44), we immediately notice that the $A_{\Phi\Phi}$ block only consists of terms that resemble a Poisson equation, for which preconditioners like Algebraic Multigrid (AMG) [19] combined with Conjugate Gradient (CG) iterations work well.

Continuing with the diagonal, the $A_{c_k c_k}$ blocks are not as simple and involve a diffusive term as well as a (usually dominant) advective term with anisotropic coefficients. In this case, classical AMG will not work well since its heuristics

require elliptic-like properties. Instead, we apply preconditioned GMRES iterations [20] to the $A_{c_k c_k}$ blocks, considering two different preconditioners. The first preconditioning approach is an additive Schwarz method (ASM) [21] where an incomplete LU factorization with 0 fill (ILU0) [22] is applied to each subdomain. The subdomains are given by the parallel decomposition of the mesh. The second approach is a Geometric Multigrid (GMG) [23] preconditioner where that same ASM-ILU0 method is used as a smoother. The coarsest grid can be solved directly with a full LU factorization. Although, naively solving the coarse grid this way does not scale to a large number processors when parallel performance is desired. Because the coarse grid and therefore the coarse discretization is usually small, even on computations with hundreds of processors, the communication between the processors is the bottleneck for performance. A solution is to redistribute and duplicate the coarse grid matrix to predefined subsets of processors. This technique performs redundant work but improves the overall solve time as shown in [24].

We choose a block-triangular preconditioner of the form

$$P = \begin{bmatrix} A_{\Phi\Phi} & & & \\ A_{c_1\Phi} & A_{c_1c_1} & & \\ \vdots & \vdots & \ddots & \\ A_{c_{m-1}\Phi} & A_{c_{m-1}c_1} & \cdots & A_{c_{m-1}c_{m-1}} \end{bmatrix}^{-1}. \quad (45)$$

Inverting a block-triangular matrix requires the inversion of the diagonal blocks, which are approximated by

$$A_{\Phi\Phi}^{-1} \approx \text{CG}(\text{AMG}(A_{\Phi\Phi})), \quad A_{c_k c_k}^{-1} \approx \text{GMRES}(\text{ASM}(A_{c_k c_k})), \quad (46)$$

in the first approach, and

$$A_{\Phi\Phi}^{-1} \approx \text{CG}(\text{AMG}(A_{\Phi\Phi})), \quad A_{c_k c_k}^{-1} \approx \text{GMRES}(\text{GMG}(A_{c_k c_k})), \quad (47)$$

in the second.

4.2. Preconditioning for high order

AMG is more memory intensive for higher-order discretizations. In this case, p -multigrid has been successful in the past [25, 26]. For the $A_{\Phi\Phi}$ block, we consider a p -multigrid strategy where AMG is applied to a lower-order p -coarsened problem. This coarsened problem uses the same DG discretization for $p = 1$, where the penalization terms are appropriately updated for the lower order. We include element-wise Jacobi as a relaxation scheme, where inter-element contributions are ignored to maintain locality.

For the concentration blocks, we consider the same additive Schwarz method described for $p = 1$. We do not consider the use of GMG for the high-order case.

The block preconditioner (45) with the described p -multigrid method for the potential block exhibits convergence issues for some numerical experiments of section 5 for $p = 3$. It is unclear to the authors why this is the case. Instead, a

different ordering of the preconditioning steps works better: solving the concentration blocks first, then the potential blocks. We theorize that the couplings are important in the low-order coarse problem but have only heuristic evidence. We thus use the following preconditioner:

$$P = \begin{bmatrix} A_{\Phi\Phi} & A_{\Phi c_1} & \cdots & A_{\Phi c_{m-1}} \\ & A_{c_1 c_1} & & \\ & \vdots & \ddots & \\ & A_{c_{m-1} c_1} & \cdots & A_{c_{m-1} c_{m-1}} \end{bmatrix}^{-1}. \quad (48)$$

Inverting this matrix only requires the inversion of the diagonal blocks, which are approximated by

$$A_{\Phi\Phi}^{-1} \approx \text{CG}(\text{PMG}(A_{\Phi\Phi})), \quad A_{c_k c_k}^{-1} \approx \text{GMRES}(\text{ASM}(A_{c_k c_k})). \quad (49)$$

4.3. Implementation

The implementation is part of the **EchemFEM** package [27]. It is realized using **fire Drake** [28] as a finite element discretization tool, which allows for automated code generation and optimization. We leverage the capability to generate kernels of tensor product finite elements [17] on quadrilateral [29] and extruded hexahedral meshes [30]. Note that the algorithms and discretization techniques presented here can also be applied to triangular and tetrahedral elements. Furthermore, **fire Drake** provides the necessary infrastructure to realize the presented GMG preconditioner [31]. The nonlinear and linear solves are handed off to the **PETSc** [32] linear algebra backend, and **BoomerAMG** [33] from the **hypr** library [34] is used for the AMG implementation. For higher-order simulations, we use **fire Drake**'s matrix-free capabilities [35]. In appendix Appendix A we provide all solver options, along with relative tolerances of each inner Krylov method, the outer FGMRES [36], and the outer Newton solver.

To help the convergence of Newton's method, we start with a constant initial guess for the concentrations using the inlet values c_k^{in} . For the potential, we obtain an initial guess by first solving the charge conservation equation with constant concentrations (a Poisson equation). For this initial potential solution, we use the solver for the potential block defined in appendix Appendix A, with a conjugate gradient tolerance of 10^{-2} .

5. Numerical results

In this section, we investigate the numerical performance of the DG scheme and preconditioning strategies. We perform a convergence test for polynomial orders $p = 1, 2, 3$ and strong scaling tests for a large parallel plate flow channel example for $p = 1$ and $p = 3$. All tests are performed in three-dimensional domains.

5.1. Convergence tests

In section 3, we established a discretization scheme based on well-known DG methods. As a first step, we have to make sure that the presented method provides the expected accuracy. Optimally, we would be able to prove an error estimate and therefore a theoretical convergence rate through analysis of (43).

Another, although less thorough, way of determining the convergence rate is by solving a manufactured problem and comparing the solution against the known analytical solution. The way the scheme was set up, we expect the convergence rate to be similar to the minimum rate of each individual treated equation. Therefore, the convergence rate of the concentration variables should be close to that of an advection-diffusion-reaction equation, i.e. $p + \frac{1}{2}$ in the advection-dominated regime [37], and the convergence rate of the potential variable should be close to that of a diffusion equation, i.e. $p + 1$ [16].

We use the nondimensional version of a two-ion system with inverse Péclet numbers $\hat{D}_1 = 5 \times 10^{-6}$ and $\hat{D}_2 = 10^{-5}$, and charge numbers $z_1 = 2$ and $z_2 = -2$. The analytical manufactured solution is chosen as

$$c_{1\text{ex}} = \cos x + \sin y + 3, \quad (50)$$

$$\Phi_{\text{ex}} = \sin x + \cos y + 3, \quad (51)$$

on the domain $\Omega \in (0, 1)^3$. All boundary conditions on $\partial\Omega$ are prescribed using the exact solutions. Additionally, a parabolic velocity profile is defined with $\mathbf{u} = (6y(1-y), 0, 0)$ in the whole domain. We choose an initial mesh size using 64 hexahedral elements with a polynomial order of $p = 1$ and compute the L^2 error norms of each variable

$$\|c_1 - c_{1\text{ex}}\|_2, \quad \|\Phi - \Phi_{\text{ex}}\|_2. \quad (52)$$

Then, we subsequently halve the element size h_e using uniform refinement. The process is repeated for polynomial orders $p = 2$ and $p = 3$. Figure 1 shows the results for this test and one can observe a convergence rate of approximately $p + 1$ for Φ . For c_1 , the rate appears to be $p + 1$ for the coarser meshes, until the later refinements reveals the asymptotic rate of $p + \frac{1}{2}$. This asymptotic rate is not reached for $p = 3$.

Looking at these results, one has to keep in mind that we determined the convergence rates on a Cartesian grid, and they might deteriorate on unstructured or curved grids [38, 39].

We now briefly investigate how the accuracy of the method relates to computational cost. For the manufactured solution problem described above, we calculate the total computational time and total L^2 error as we vary the size of the problem. The total error is the sum of the concentration and potential errors. On an Intel 18-core Xeon E5-2695 v4 architecture with 2.1 GHz clock speed, we use two nodes and a total of 64 processors. For $p = 1$, we use the preconditioner described in section 4.1 with the additive Schwarz method for the concentration blocks, and for $p = 3$ we use the preconditioner for high order described in section 4.2.

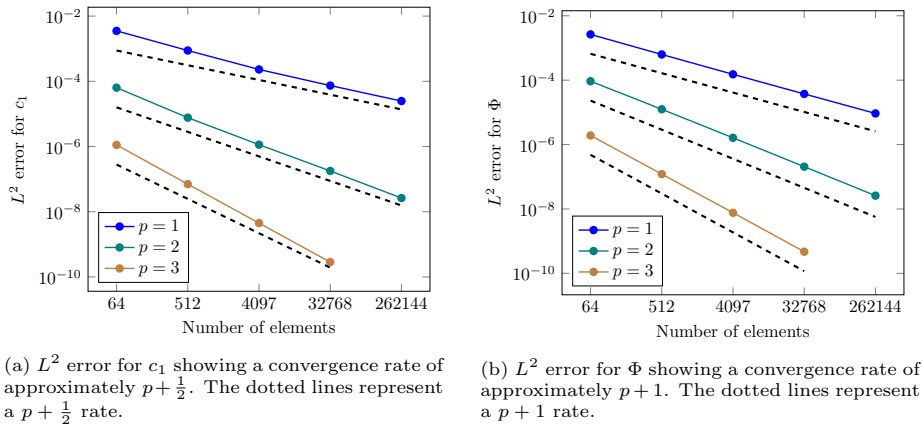


Figure 1: Convergence tests for the manufactured solution.

Table 1: Computational time and total L^2 errors for varying problem sizes of the toy problem.

# DoFs	$p = 1$		$p = 3$	
	CPU time (s)	L^2 error	CPU time (s)	L^2 error
65,536	15.31	3.84×10^{-4}	29.92	1.92×10^{-7}
524,288	18.17	1.14×10^{-4}	41.18	1.12×10^{-8}
4,194,304	34.95	3.40×10^{-5}	111.3	7.61×10^{-10}
33,554,432	209.1	9.82×10^{-6}	-	-

In table 1, we provide computational timings and total L^2 errors for $p = 1$ and $p = 3$ as we vary the problem size. We note that the computational resources are fixed so there is insufficient memory for the largest high-order case. Additionally, the first row of results is around a thousand degrees of freedom per processor, which is not typically cost-efficient. Even so, the smallest $p = 3$ problem is twice as accurate and seven times faster than the largest $p = 1$ problem. It is evident that increasing polynomial order is preferable to mesh refinement when seeking high accuracy results.

5.2. Parallel plate flow channel

We consider a 3D extension of the parallel plate reactor from [7]. A schematic of the reactor is given in figure 2. The distance between the two electrodes is $h = 0.01$ m, and their length is $L = 0.02$ m. The inlet and outlet regions included in the domain are of length $L_a = L_b = 0.05$ m, and the channel has a width $w = 0.06$ m.

The velocity field $\mathbf{u} = (u_x, u_y, u_z)$ in the reactor is given by the parabolic profile

$$u_x = \frac{6u_{\text{avg}}}{h^2}y(h - y), \quad u_y = u_z = 0. \quad (53)$$

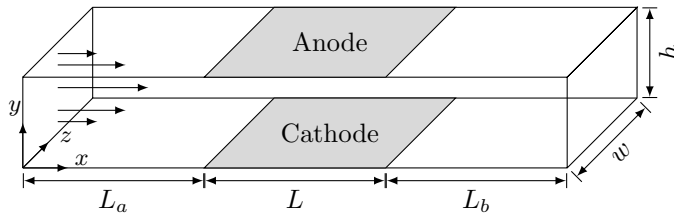


Figure 2: Parallel plate reactor diagram.

Choosing zero-Neumann boundary conditions on xy -faces means that the channel is periodic in the z -direction. For this test case, we choose $u_{\text{avg}} = 0.03 \text{ m s}^{-1}$.

We consider the three-ion system from [7] with an electrolyte solution consisting of 0.01 M CuSO_4 and $1.0 \text{ M H}_2\text{SO}_4$. The ions are H^+ , Cu^{2+} , and SO_4^{2-} with properties given in table 2. This results in average Péclet numbers, $u_{\text{avg}} \frac{h}{D_k}$, of 3.22×10^4 , 4.17×10^5 , and 2.82×10^5 for H^+ , Cu^{2+} , and SO_4^{2-} , respectively.

Table 2: Physical parameters of the ions for the parallel plate flow reactor.

Ion	Diffusion coefficient (m^2s^{-1})	Inlet concentration (M)	charge
Cu^{2+}	7.20×10^{-10}	0.01	2
SO_4^{2-}	10.65×10^{-10}	1.01	-2
H^+	93.12×10^{-10}	2.0	1

At the electrodes, the electrochemical reaction is given by the Butler-Volmer equation (9) for the reacting ion, Cu^{2+} , and no reaction for the other ions. The parameters for the Butler-Volmer equation are $\gamma = 1$, $\alpha_1 = \alpha_2 = 0.5$, $T = 298.15 \text{ K}$, $n = 2$, and $c_{\text{Cu}^{2+}}^*$ is given by the inlet concentration of Cu^{2+} in table 2. The applied potential Φ_{app} is zero at the anode and 0.03 V at the cathode. For this redox reaction, Cu^{2+} is the oxidant, and the solid copper of the electrode is the reductant (with constant concentration). To introduce variations in the z direction, we consider the following parabolic profile for the exchange current density:

$$J_0 = \frac{3}{5} \bar{J}_0 \left[2 - \left(\frac{z - w/2}{w/2} \right)^2 \right], \quad (54)$$

which has an average of $\bar{J}_0 = 30 \text{ A m}^{-2}$ over the width of the channel.

We first use a structured hexahedral mesh such that, in the xy -plane, elements are concentrated in the electrode region as illustrated in figure 3, and elements are equally spaced in the z -plane. The coarse mesh of $64 \times 16 \times 8$ elements is uniformly refined three times, resulting in a mesh with 4,194,304 elements. Note that this mesh has elements with large aspect ratios.

We also consider a mesh where the xy -plane is an unstructured mesh as illustrated in figure 4. Similarly to the structured mesh, the coarse 2D mesh is

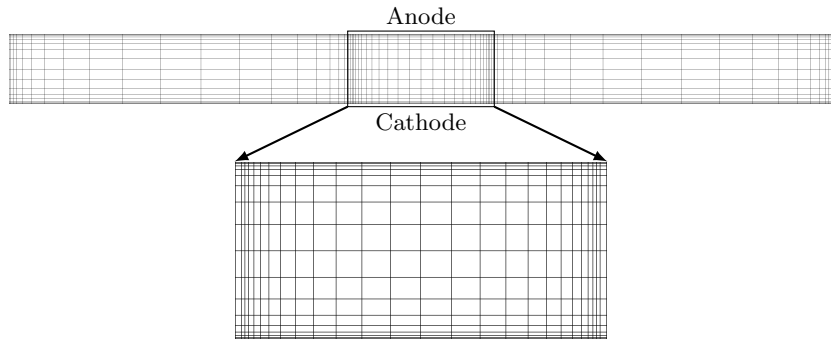


Figure 3: Cross-section of the coarse mesh in the xy -plane and zoom-in of the electrode region.

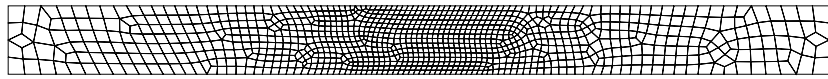


Figure 4: Cross-section of the unstructured coarse mesh in the xy -plane.

extruded in the z -direction with eight equally-spaced elements. After uniformly refining three times, we obtain a mesh with 4,153,344 elements.

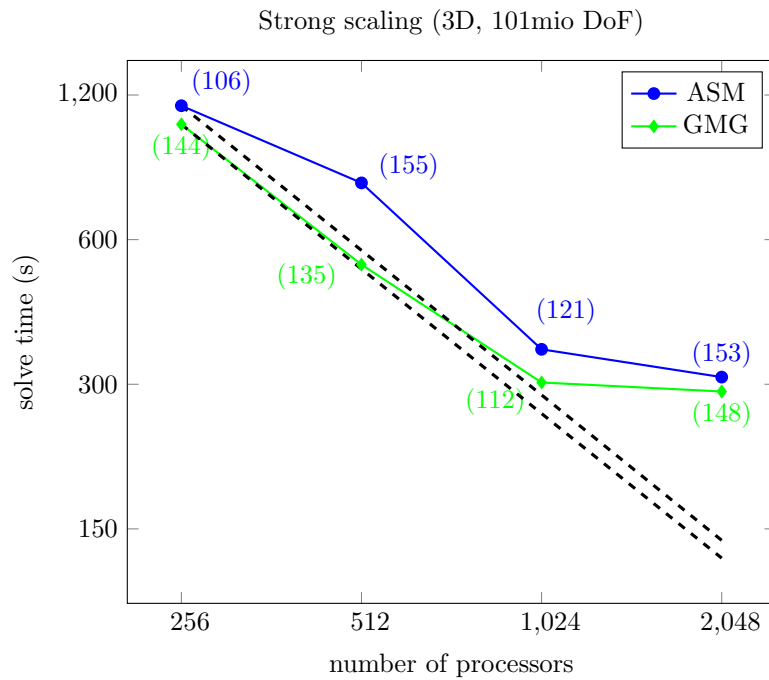


Figure 5: Strong scaling timings for the parallel flow plane channel for $p = 1$. The total number of outer GMRES iterations are given in parentheses.

We now investigate the strong scaling of the preconditioners for the parallel flow plane channel. The experiments are performed on an Intel 18-core Xeon E5-2695 v4 architecture with 2.1 GHz clock speed. Using elements of $p = 1$ polynomial order results in 100,663,296 degrees of freedom for the structured mesh, and 99,680,256 degrees of freedom for the unstructured mesh.

We begin with 256 processors (on 8 nodes) and successively double the number of processors and nodes. In figure 5, we illustrate the strong scaling results for both preconditioning approaches described in section 4 on the structured mesh described above, and in figure 6 on the unstructured mesh. ASM refers to using the additive Schwarz method with ILU0 on the subdomains as a preconditioner for the concentration blocks, while GMG refers to using a geometric multigrid method with that same ASM as a smoother. For both ASM and GMG, we present solution times and the total number of outer FGMRES iterations. In each case, four Newton iterations are required to reach the prescribed tolerance.

First, we discuss the scaling results for the unstructured mesh in figure 5. We observe that, overall, ASM is the more expensive method. Further investigation of the iteration counts of the inner GMRES used for the concentration blocks reveals that GMG only takes a few iterations, while ASM often takes around 50-100 iterations (sub-iterations not shown here). Now, in terms of scaling, ASM scales almost linearly until 2,048 processors. However, it is expected that ASM becomes a weaker preconditioner as the number of subdomains increases. For GMG, the scaling is close to being linear from 256 to 1,024 processors. Naturally, the direct solver used for the coarse problem of GMG does not scale linearly and eventually dominates the computational cost at 2,048 processors. Note that there is a decrease in iterations at 512 and 1,024 processors, which may be due to how the mesh is partitioned, thus increasing the performance of the smoother and the apparent quality of the scaling. Recall that we do not have control over the domain decomposition, which in general will not be ideal. In particular, the criticality of the electrode regions should be considered in a more controlled mesh partition.

Now we compare the scaling results for the unstructured mesh in figure 6. We observe that both methods have similar almost-linear scaling, with a bump in cost at 2,048 processors. Differently from the structured mesh case, ASM is the least expensive method. In fact, the GMRES iteration count for the concentration blocks for ASM are lower in this case, typically less than 30 (sub-iterations not shown here). The structured mesh has some elements with very large aspect ratio. This could affect the conditioning of the mesh, resulting in larger number of iterations. We note that the outer GMRES iterations is also lower for the unstructured case.

Finally, we look at the scaling results for $p = 3$ and the preconditioning strategy described in section 4.2. We note that the p -multigrid method used for the potential block performs poorly on meshes with high element aspect ratios such as the ones used above. The scaling tests are therefore performed on a mesh with moderate aspect ratios. The width of the channel is changed to $w = 0.01$ m. We consider an unstructured coarse mesh similar to the one

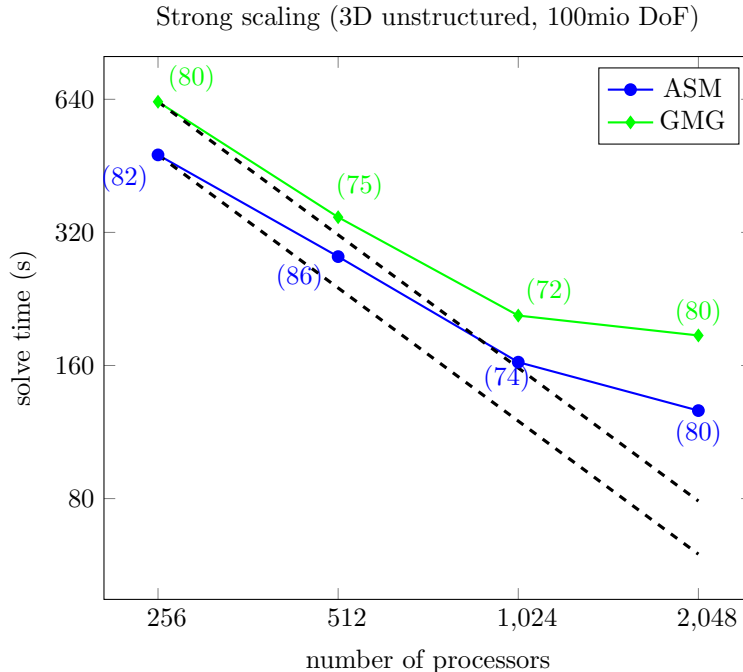


Figure 6: Strong scaling timings for the parallel flow plane channel for $p = 1$. The total number of outer GMRES iterations are given in parentheses.

illustrated in figure 4 but with slightly larger elements and extrude it in the z -direction with 6 elements. For $p = 3$, we uniformly refine the mesh 2 times for a total of 254,208 elements. One more refinement gives 2,033,664 elements, which is used for $p = 1$. Both problems consist of 48,807,936 degrees of freedom.

We display the high-order scaling results in figure 7. We observe that the scaling for $p = 3$ is about order 0.5, i.e. the cost is halved after quadrupling the number of processors. The computational timings for the smallest case is more than four times higher for $p = 3$ than $p = 1$. Nevertheless, this figure does not take into account the numerical accuracy of the results. Indeed, we recall from table 1 that higher accuracy can be obtained for higher-order problems of much smaller sizes. Strong scaling for $p = 1$ as at best linear, but increasing the polynomial order results in an exponential increase in accuracy.

6. Conclusion

In this work, we propose a high-order Discontinuous Galerkin (DG) scheme and block preconditioners for the electroneutral Nernst-Planck equations. We choose a model formulation where the electroneutrality condition is substituted to obtain a charge conservation equation. In the DG scheme, this equation is treated as an elliptic equation for the electrical potential, whereas in the mass

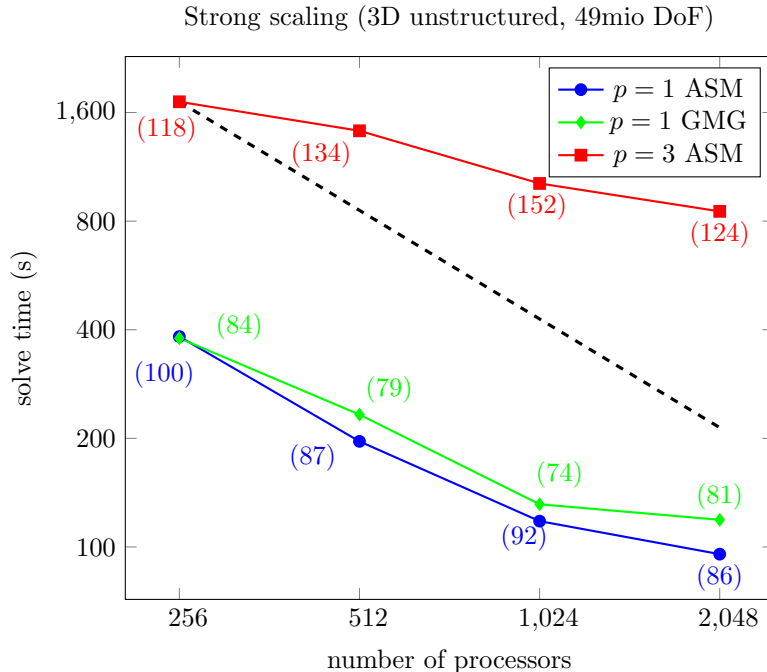


Figure 7: Strong scaling timings for the parallel flow plane channel with ASM. The total number of outer GMRES iterations are given in parentheses.

conservation equations, an upwind scheme is used for the combined advection-migration term. In numerical convergence tests, the scheme exhibits a $p + 1$ order of convergence for the potential and a $p + \frac{1}{2}$ order of convergence for the concentrations.

For $p = 1$, both proposed block preconditioners use Algebraic Multigrid for the potential block whereas an Additive Schwarz method with ILU is used for the concentration blocks, by itself or as a smoother for a Geometric Multigrid method (GMG). While both methods exhibit decent strong scaling, the GMG-based approach is less expensive on the structured mesh, although its scaling is limited by the direct solver used for the coarse grid solution. For higher order, a p -multigrid method is used for the potential block, where Algebraic Multigrid is applied to the lower-order coarsened problem. The strong scaling is less than linear in the high-order case.

For future extensions, coupling this solver with fluid dynamics is of particular interest. The Stokes or incompressible Navier-Stokes equations are relevant for flow reactors as well as the pore-scale of porous electrode systems. On the larger length scale, Darcy flow is appropriate for porous electrodes, and its multiphase extension for gas-diffusion electrodes (GDE).

Further work is needed for preconditioning in the case where electrolyte bulk reactions are present, where reaction rate constants can vary wildly. Porous

electrodes are also interesting since cathodic/anodic reactions occur throughout the domain rather than as boundary conditions.

Acknowledgments

The authors would like to thank Pablo Brubeck for his help on implementing p -multigrid. This work was performed under the auspices of the U.S. Department of Energy by Lawrence Livermore National Laboratory under Contract DE-AC52-07NA27344 and was supported by the LLNL-LDRD program under project numbers 19-ERD-035 and 22-SI-006. LLNL Release Number LLNL-JRNL-829967.

References

- [1] S. Chu, A. Majumdar, Opportunities and challenges for a sustainable energy future, *Nature* 488 (7411) (2012) 294–303. doi:10.1038/nature11475.
- [2] S. Chu, Y. Cui, N. Liu, The path towards sustainable energy, *Nature Materials* 16 (1) (2016) 16–22. doi:10.1038/nmat4834.
- [3] T. M. Gür, Review of electrical energy storage technologies, materials and systems: challenges and prospects for large-scale grid storage, *Energy & Environmental Science* 11 (10) (2018) 2696–2767. doi:10.1039/c8ee01419a.
- [4] J. W. Ager, A. A. Lapkin, Chemical storage of renewable energy, *Science* 360 (6390) (2018) 707–708. doi:10.1126/science.aat7918.
- [5] J. Newman, K. E. Thomas-Alyea, *Electrochemical systems*, John Wiley & Sons, 2012.
- [6] E. J. Dickinson, J. G. Limon-Petersen, R. G. Compton, The electroneutrality approximation in electrochemistry, *Journal of Solid State Electrochemistry* 15 (7-8) (2011) 1335–1345. doi:10.1007/s10008-011-1323-x.
- [7] L. Bortels, J. Deconinck, B. Van Den Bossche, The multi-dimensional upwinding method as a new simulation tool for the analysis of multi-ion electrolytes controlled by diffusion, convection and migration. Part 1. Steady state analysis of a parallel plane flow channel, *Journal of Electroanalytical Chemistry* 404 (1) (1996) 15–26. doi:10.1016/0022-0728(95)04371-3.
- [8] G. Bauer, A coupled finite element approach for electrochemical systems, Ph.D. thesis, Technische Universität München (2012).
- [9] H. Liu, Z. Wang, A free energy satisfying discontinuous Galerkin method for one-dimensional Poisson–Nernst–Planck systems, *Journal of Computational Physics* 328 (2017) 413–437. doi:10.1016/j.jcp.2016.10.008.

- [10] Z. Sun, J. A. Carrillo, C.-W. Shu, A discontinuous Galerkin method for nonlinear parabolic equations and gradient flow problems with interaction potentials, *Journal of Computational Physics* 352 (2018) 76–104. doi:10.1016/j.jcp.2017.09.050.
- [11] R. Hartmann, T. Leicht, Higher order and adaptive DG methods for compressible flows, *37th Advanced CFD Lecture Series: Recent developments in higher order methods and industrial application in aeronautics 2014* (3) (2014) 1–156.
- [12] A. J. Wathen, Preconditioning, *Acta Numerica* 24 (2015) 329–376. doi:10.1017/s0962492915000021.
- [13] B. Rivière, *Discontinuous Galerkin methods for solving elliptic and parabolic equations: theory and implementation*, SIAM, 2008. doi:10.1137/1.9780898717440.
- [14] F. Brezzi, L. D. Marini, E. Süli, Discontinuous Galerkin methods for first-order hyperbolic problems, *Mathematical models and methods in applied sciences* 14 (12) (2004) 1893–1903. doi:10.1142/s0218202504003866.
- [15] B. Cockburn, C.-W. Shu, Runge–Kutta discontinuous Galerkin methods for convection-dominated problems, *Journal of scientific computing* 16 (3) (2001) 173–261. doi:10.1007/1-84628-205-5_5.
- [16] D. N. Arnold, F. Brezzi, B. Cockburn, L. D. Marini, Unified analysis of discontinuous Galerkin methods for elliptic problems, *SIAM journal on numerical analysis* 39 (5) (2002) 1749–1779. doi:10.1137/s0036142901384162.
- [17] A. T. T. McRae, G.-T. Bercea, L. Mitchell, D. A. Ham, C. J. Cotter, Automated generation and symbolic manipulation of tensor product finite elements, *SIAM Journal on Scientific Computing* 38 (5) (2016) S25–S47. doi:10.1137/15M1021167.
- [18] J. E. Dennis Jr, R. B. Schnabel, *Numerical methods for unconstrained optimization and nonlinear equations*, SIAM, 1996.
- [19] J. W. Ruge, K. Stüben, Algebraic multigrid, in: *Multigrid methods*, Vol. 3 of *Frontiers in Applied Mathematics*, SIAM, Philadelphia, 1987, Ch. 4, pp. 73–130. doi:10.1137/1.9781611971057.ch4.
- [20] Y. Saad, M. H. Schultz, GMRES: A generalized minimal residual algorithm for solving nonsymmetric linear systems, *SIAM Journal on Scientific and Statistical Computing* 7 (3) (1986) 856–869. doi:10.1137/0907058.
- [21] O. Widlund, M. Dryja, An additive variant of the Schwarz alternating method for the case of many subregions, *Tech. rep.* (1987).

- [22] J. A. Meijerink, H. A. van der Vorst, An iterative solution method for linear systems of which the coefficient matrix is a symmetric M-matrix, *Mathematics of Computation* 31 (137) (1977) 148–162. doi:10.1090/s0025-5718-1977-0438681-4.
- [23] A. Brandt, Multi-level adaptive solutions to boundary-value problems, *Mathematics of Computation* 31 (138) (1977) 333–390. doi:10.1090/s0025-5718-1977-0431719-x.
- [24] D. A. May, P. Sanan, K. Rupp, M. G. Knepley, B. F. Smith, Extreme-scale multigrid components within PETSc, in: *Proceedings of the Platform for Advanced Scientific Computing Conference, PASC '16*, Association for Computing Machinery, New York, NY, USA, 2016. doi:10.1145/2929908.2929913.
- [25] K. J. Fidkowski, T. A. Oliver, J. Lu, D. L. Darmofal, p -multigrid solution of high-order discontinuous Galerkin discretizations of the compressible navier–stokes equations, *Journal of Computational Physics* 207 (1) (2005) 92–113. doi:10.1016/j.jcp.2005.01.005.
- [26] B. Helenbrook, D. Mavriplis, H. Atkins, Analysis of “ p ”-multigrid for continuous and discontinuous finite element discretizations, in: *16th AIAA Computational Fluid Dynamics Conference*, 2003, p. 3989.
- [27] T. Roy, J. Andrej, V. Beck, V. Ehlinger, N. Govindarajan, T. Lin, LLNL/echemfem: EchemFEM (Dec. 2022). doi:10.5281/zenodo.7384450.
- [28] F. Rathgeber, D. A. Ham, L. Mitchell, M. Lange, F. Luporini, A. T. T. McRae, G.-T. Bercea, G. R. Markall, P. H. J. Kelly, Firedrake: automating the finite element method by composing abstractions, *ACM Trans. Math. Softw.* 43 (3) (2016) 24:1–24:27. doi:10.1145/2998441.
- [29] M. Homolya, D. A. Ham, A parallel edge orientation algorithm for quadrilateral meshes, *SIAM Journal on Scientific Computing* 38 (5) (2016) S48–S61. doi:10.1137/15M1021325.
- [30] G. Bercea, A. T. T. McRae, D. A. Ham, L. Mitchell, F. Rathgeber, L. Nardi, F. Luporini, P. H. J. Kelly, A structure-exploiting numbering algorithm for finite elements on extruded meshes, and its performance evaluation in Firedrake, *Geoscientific Model Development* 9 (10) (2016) 3803–3815. doi:10.5194/gmd-9-3803-2016.
- [31] L. Mitchell, E. H. Müller, High level implementation of geometric multigrid solvers for finite element problems: applications in atmospheric modelling, *Journal of Computational Physics* 327 (2016) 1–18. doi:10.1016/j.jcp.2016.09.037.

- [32] S. Balay, W. D. Gropp, L. C. McInnes, B. F. Smith, Efficient management of parallelism in object oriented numerical software libraries, in: E. Arge, A. M. Bruaset, H. P. Langtangen (Eds.), *Modern Software Tools in Scientific Computing*, Birkhäuser Press, 1997, pp. 163–202.
- [33] V. E. Henson, U. M. Yang, BoomerAMG: A parallel algebraic multigrid solver and preconditioner, *Appl. Numer. Math.* 41 (1) (2002) 155–177. doi:10.1016/S0168-9274(01)00115-5.
- [34] hypre: High performance preconditioners, <https://computation.llnl.gov/projects/hypre-scalable-linear-solvers-multigrid-methods>.
- [35] R. C. Kirby, L. Mitchell, Solver composition across the PDE/linear algebra barrier, *SIAM Journal on Scientific Computing* 40 (1) (2018) C76–C98. doi:10.1137/17M1133208.
- [36] Y. Saad, A flexible inner-outer preconditioned GMRES algorithm, *SIAM Journal on Scientific Computing* 14 (2) (1993) 461–469. doi:10.1137/0914028.
- [37] B. Ayuso, L. D. Marini, Discontinuous Galerkin methods for advection-diffusion-reaction problems, *SIAM Journal on Numerical Analysis* 47 (2) (2009) 1391–1420. doi:10.1137/080719583.
- [38] B. Cockburn, B. Dong, J. Guzmán, Optimal convergence of the original DG method for the transport-reaction equation on special meshes, *SIAM Journal on Numerical Analysis* 46 (3) (2008) 1250–1265. doi:10.1137/060677215.
- [39] G. R. Richter, An optimal-order error estimate for the discontinuous Galerkin method, *Mathematics of Computation* 50 (181) (1988) 75–88. doi:10.1090/s0025-5718-1988-0917819-3.

Appendix A. Solver parameters

Here we provide PETSc options used to construct the solvers described in section 4. The parameters used for the $p = 1$ case are provided in listing 1, and for $p > 1$ in listing 2.

Listing 1: Solver options for the discretized electrochemical system for $p = 1$.

```

1 | "snes_type": "newton",
2 | "snes_rtol": 1E-6,
3 | "ksp_type": "fgmres",
4 | "ksp_rtol": 1E-3,
5 | "pc_type": "fieldsplit",
6 | % For the potential block
7 | "fieldsplit_0": {
8 |     "ksp_rtol": 1E-1,
9 |     "ksp_type": "cg",

```



```

10     "pc_type": "hypre",
11     "pc_hypre_boomeramg": {
12         "strong_threshold": 0.7,
13         "coarsen_type": "HMIS",
14         "agg_n1": 3,
15         "interp_type": "ext+i",
16         "agg_num_paths": 5,
17     },
18 },
19 % For each concentration block k, using the ASM preconditioner:
20 "fieldsplit_[k]": {
21     "ksp_rtol": 1E-1,
22     "ksp_type": "gmres",
23     "pc_type": "asm",
24     "sub_pc_type": "ilu",
25 },
26 % Otherwise, for each concentration block k, using the GMG preconditioner:
27 "fieldsplit_[k]": {
28     "ksp_rtol": 1E-1,
29     "ksp_type": "gmres",
30     "pc_type": "mg",
31     "mg_levels_ksp_type": "richardson",
32     "mg_levels_pc_type": "asm",
33     "mg_levels_sub_pc_type": "ilu",
34     "mg_coarse": {
35         "pc_type": "python",
36         "pc_python_type": "firedrake.AssembledPC",
37         "assembled": {
38             "mat_type": "aij",
39             "pc_type": "telescope",
40             "pc_telescope_reduction_factor": REDFACTOR,
41             "pc_telescope_subcomm_type": "contiguous",
42             "telescope_pc_type": "lu",
43             "telescope_pc_factor_mat_solver_type": "mumps"
44         }
45     },
46 }

```

Listing 2: Solver options for the discretized electrochemical system for $p > 1$.

```

1 | "mat_type": "matfree",
2 | "snes_type": "newton",
3 | "snes_rtol": 1E-6,
4 | "ksp_type": "fgmres",
5 | "ksp_rtol": 1E-3,
6 | "pc_type": "fieldsplit",
7 | % For the potential block
8 | "fieldsplit_[m]": {
9 |     "ksp_rtol": 1E-1,
10 |    "ksp_type": "cg",
11 |    "pc_type": "python",
12 |    "mat_type": "matfree",
13 |    "pc_python_type": __name__+".CoarsenPenaltyPMGPC",
14 |    "pmg_mg_levels_ksp_type": "chebyshev",
15 |    "pmg_mg_levels_ksp_max_it": 4,
16 |    "pmg_mg_levels_ksp_norm_type": "unpreconditioned",
17 |    "pmg_mg_levels_": {
18 |        "pc_type": "python",

```

```

19         "pc_python_type": __name__ + "." + "CellIntegralPC",
20         "assembled_pc_type": "jacobi",
21     },
22     "pmg_coarse_mat_type": "aij",
23     "pmg_mg_coarse": {
24         "ksp_type": "cg",
25         "ksp_rtol": 1e-3,
26         "pc_type": "hypre",
27     },
28     },
29 % For each concentration block k, using the ASM preconditioner:
30 "fieldsplit_[k-1]": {
31     "ksp_rtol": 1E-1,
32     "ksp_type": "gmres",
33     "pc_type": "python",
34     "pc_python_type": "firedrake.AssembledPC",
35     "assembled": {
36         "pc_type": "asm",
37         "pc_asm_overlap": 1,
38         "sub_pc_type": "ilu"
39     },
40 },

```

The reduction factor `REDFACTOR` for the coarse grid redistribution is chosen depending on the number of processors such that the solver sub-communicator always includes exactly 8 nodes. The default overlap for ASM is one element.

The custom preconditioner `CoarsenPenaltyPMGPC` is p -multigrid with $p = 1$ on the coarse level where the proper penalization parameters are used for the DG discretization. The custom preconditioner `CellIntegralPC` is used to ignore inter-element contributions. These custom solvers are available in the `EchemFEM` package [27].